




RESEARCH ARTICLE | NOVEMBER 07 2024

Investigating the effect of dynamic laser beam oscillations in remote fusion cutting process

Special Collection: [Proceedings of the International Congress of Applications of Lasers & Electro-Optics \(ICALEO 2024\)](#)

Matteo Busatto  ; Leonardo Caprio  ; Barbara Previtali 

 Check for updates

J. Laser Appl. 36, 042068 (2024)
<https://doi.org/10.2351/7.0001599>



Articles You May Be Interested In

Laser remote-fusion cutting with solid-state lasers

J. Laser Appl. (July 2013)

Optimization of circular scan path to produce bowl shapes in 3D laser forming process

J. Laser Appl. (September 2017)

Ultrafast pulsed laser high precision micromachining of rotational symmetric parts

J. Laser Appl. (February 2021)

ALIA THE LASER INSTITUTE **Journal of Laser Applications** [Learn More](#)

- RAPID TIME TO ACCEPTANCE**
- COMMUNITY DRIVEN**
- EXPANSIVE COVERAGE**
- PRESTIGIOUS EDITORIAL BOARD**
- EXTENSIVE MARKETING**

Investigating the effect of dynamic laser beam oscillations in remote fusion cutting process

Cite as: J. Laser Appl. 36, 042068 (2024); doi: 10.2351/7.0001599

Submitted: 1 July 2024 · Accepted: 20 October 2024 ·

Published Online: 7 November 2024



Matteo Busatto,  Leonardo Caprio,  and Barbara Previtali 

AFFILIATIONS

Department of Mechanical Engineering, Politecnico di Milano, Via La Masa 1, Milan 20156, Italy

Note: Paper published as part of the special topic on Proceedings of the International Congress of Applications of Lasers & Electro-Optics 2024.

ABSTRACT

The latest research on laser beam fusion cutting has revealed significant improvements in process productivity and cut quality through the use of dynamic beam shaping techniques. While many studies have investigated dynamic beam shaping for proximity cutting, the influence of laser beam oscillations on the remote fusion cutting process remains unexplored. The present work aims to study the effect of dynamic beam shaping on the remote fusion cutting process through analytical modeling, experimental investigations, and *in situ* high-speed monitoring. Initially, an analytical model based on thermodynamic analysis was developed to assess the influence of circular oscillations on the process zone. This model facilitates the evaluation of process performance from an energetic perspective, providing an estimate of the maximum achievable cutting speed for the remote fusion cutting process across various operating conditions. A significant increment in process productivity could be achieved through beam oscillations. Furthermore, based on theoretical findings, the effect of circular laser beam oscillations superimposed on the processing feed direction was experimentally investigated using a 1 mm thick AISI304 stainless steel material. A 6 kW fiber laser was utilized, alongside a high-speed camera-based system for *in situ* process monitoring. The experimental results demonstrate a significant increase in the process productivity under dynamic beam shaping conditions, consistent with theoretical findings. Specifically, the maximum achievable cutting speed could be increased from 0.13 to 0.20 m/s. Furthermore, the cut quality of produced samples was evaluated in terms of kerf morphology and profile.

Key words: laser cutting, stainless steel, high speed imaging, remote cutting, beam shaping

© 2024 Author(s). All article content, except where otherwise noted, is licensed under a Creative Commons Attribution (CC BY) license (<https://creativecommons.org/licenses/by/4.0/>). <https://doi.org/10.2351/7.0001599>

I. INTRODUCTION

Today, laser cutting of metal materials stands out as one of the prevalent applications in the manufacturing industry. Conventionally, the separation of metal materials relies on the combined use of a high-intensity laser beam and a high-pressure gas jet, arranged coaxially and operating in close proximity to the workpiece.^{1,2} The laser beam melts the metal, while an inert gas jet expels the molten material from the cutting kerf. In the absence of an external gas and its blowing action, the laser may operate from a distance, resulting in a remote cutting configuration.³ Instead of utilizing high-pressure gas to expel the molten material, the remote fusion cutting process relies on a single-pass removal mechanism driven by partial vaporization and downward melt ejection induced by vapor recoil pressure.⁴

To date, only a few publications have addressed remote fusion cutting process in terms of productivity and part quality. Antonova *et al.* investigated the remote cutting of steel plates with CO₂ laser,⁵ while the effect of pulsed emission was discussed by Gladush and Rodionov.⁶ Lütke *et al.* compared the performance of remote fusion cutting for different material thicknesses using a fiber laser source.^{7,8} The influence of process parameters on the cutting front angle was addressed by Schober.⁹ On the other hand, the impact of the laser beam incident angle on process performances was investigated by Villumsen and Kristiansen for the processing of stainless steel plates.¹⁰ A detailed analysis on cut quality for different materials was performed by Pihlava *et al.* in terms of kerf width, roughness, perpendicularity, cut-edge sharpness, and burr height.¹¹ Furthermore, theoretical models of the

18 November 2024 10:36:43

process dynamics were proposed by Matti *et al.*¹² and Kristiansen *et al.*¹³

Remote cutting offers numerous advantages for processing thin materials, such as the reduced risk of tool collision, elimination of cutting gas usage, narrower access paths, and increased accessibility due to the ability to operate at a distance. However, its adoption in the industrial field remains limited. This is primarily due to the significantly lower processing speeds compared to conventional fusion and reactive cutting processes. However, recent advancements in laser cutting techniques utilizing novel beam shaping methods have demonstrated substantial improvements in processing speed and part quality. These techniques refer to the manipulation of laser beam characteristics to achieve a desired beam profile and intensity distribution.

Latest research from KU Leuven and IWS Dresden has revealed notable improvements in terms of process productivity and part quality, for the fusion cutting of high-thickness materials by employing dynamic beam shaping (DBS) techniques.¹⁴ These approaches rely on the high speed motion of laser beam, superimposed to the cutting direction. Laser oscillations around the kerf enable to shape the interaction zone into an arbitrary geometry while preserving the beam intensity distribution. Goppold *et al.* investigated the effects of different laser oscillation patterns on the part quality of high-thick stainless steel plates by employing a high-dynamic scanner system^{15,16} and a tip-tilt piezo platform mirror.¹⁷ Studies by Levichev *et al.* have demonstrated significant improvements in the part quality of 12 mm thick mild and stainless steel employing longitudinal linear oscillations.^{18,19} Thermal monitoring and high-speed imaging of the cutting process were introduced by Kardan *et al.*^{20,21} for evaluating the process dynamics, focusing on the impact of oscillation amplitude and frequency on the workpiece temperature and melt flow behavior.

Although significant improvements of process performances have been demonstrated for fusion cutting of thick metal materials, to date, the application of beam shaping techniques for the remote fusion cutting process has been scarcely explored in the literature,^{22,23} while the impact of laser beam oscillations has never been addressed.

The scope of this work is to explore the effect of dynamic beam shaping on the remote fusion cutting process. Initially, an analytical model based on thermodynamic analysis was developed to evaluate process performance from an energetic perspective. This provides an estimate of the maximum achievable cutting speed for the remote fusion cutting process across various operating conditions. Furthermore, the effect of circular laser beam oscillations superimposed to the processing feed direction was experimentally investigated. A 6 kW fiber laser source was employed for the remote cutting of 1 mm thick stainless steel AISI304, which represents one of the most commonly used material and thickness in industrial remote cutting applications. Moreover, a high-speed camera-based system for *in situ* process monitoring was used to observe the melt dynamics.

II. MODELING

An analytical model for estimating the maximum achievable cutting speed during the remote fusion cutting process was

developed based on the thermodynamic model presented by Steen and Mazumder.²⁴ According to the proposed energy balance approach, the absorbed laser power P_{abs} required to melt the volume of material necessary for generating a cutting kerf can be derived as

$$P_{abs} = P \cdot A = Fv\rho [c_p\Delta T + h_s + f_v h_v], \quad (1)$$

where P is the average power delivered by the laser source, A is the absorptivity coefficient, F is the cross-sectional area of the cutting kerf, ΔT is the solidus temperature variation, ρ is the material density, c_p is the specific heat capacity, h_s and h_v are the latent heat of fusion and vaporization, respectively, while f_v is the fraction of vaporized melt.

From Eq. (1), it is evident that the absorbed laser power P_{abs} can be estimated by calculating the absorptivity coefficient A and the rate of molten material per unit time, which is related to the cross-sectional area F , for the specific material of interest.

By approximating the cutting front with an inclined plane, as schematically illustrated in Fig. 1(a), and disregarding multiple reflections within the cutting kerf, the absorptivity coefficient A can be expressed by the Fresnel equation. This equation determines the coefficient as a function of laser beam incident angle θ on the cutting front. Based on the Fresnel equations, the laser reflectivity R varies according to material properties, angle of incidence, and polarization state of the radiation.

The average angle of incidence at the maximum cutting speed [Fig. 1(a)] can be computed according to Mahrle and Beyer,²⁵ while the contributions from parallel and perpendicular polarization states can be computed as

$$R_p = \frac{[n \cdot \cos(\theta) - 1]^2 + [k \cdot \cos(\theta)]^2}{[n \cdot \cos(\theta) + 1]^2 + [k \cdot \cos(\theta)]^2}, \quad (2)$$

$$R_s = \frac{[n - \cos(\theta)]^2 + k^2}{[n + \cos(\theta)]^2 + k^2}, \quad (3)$$

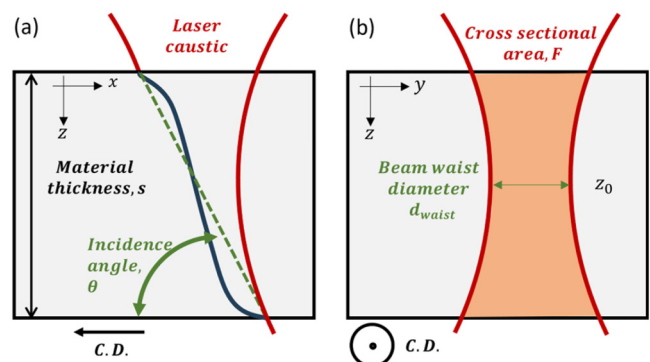


FIG. 1. (a) Cutting front and angle of incidence, θ , for the maximum achievable cutting speed and (b) cross-sectional area, F , of the cutting kerf.

18 November 2024 10:36:43

TABLE I. Stainless steel AISI304: chemical composition (wt. %).

C	Mn	Si	P	S	Cr	Ni	N	Fe
0.07	2	1	0.05	0.02	19	10.5	0.11	balance

where $n + ik$ is the material complex refractive index. For unpolarized laser radiation, the overall reflectivity is calculated as the average value of the two contributions and the absorptivity can be expressed as

$$A = 1 - R = 1 - \frac{R_S + R_P}{2}. \quad (4)$$

Moreover, an analytical expression for the cross-sectional area F was proposed by Lind *et al.*²⁶ Considering Fig. 1(b), they showed that the cross-sectional area of the cutting kerf can be approximated as the area covered by the beam caustic in the plane transversal to the feeding direction,

$$F = \int_{z=0}^{z=s} \left[d_{\text{waist}} \cdot \sqrt{1 + \frac{(z - z_0)^2}{z_R^2}} \right] dz, \quad (5)$$

where d_{waist} is the laser beam waist diameter at z_0 axial position and z_R is the Rayleigh length.

It is worth noticing that the laser beam diameter $d(z)$ influences both the cross-sectional area of the kerf, F , and the absorptivity A , having a significant impact on the estimated absorbed laser power.

Furthermore, a fraction of the laser power absorbed by the workpiece dissipates through heat conduction phenomena, which does not contribute to the melting process. An analytical expression of these power losses was provided by Schulz *et al.*²⁷ as

$$P_L = 4 \cdot K_c \cdot s \cdot \Delta T \cdot \left[\frac{Pe}{2} \right]^{0.3}, \quad (6)$$

where K_c is the thermal conductivity, s is the material thickness, and Pe is the Peclet number expressed as

TABLE II. Stainless steel AISI304: physical properties.

Physical Properties	Values
Complex refractive index, $n + ki$	3.6–5.0i
Solidus temperature, T_{solidus} (K)	1670
Material density, ρ_{liquid} (kg m^{-3})	6900
Heat capacity, $c_{p,\text{liquid}}$ ($\text{J kg}^{-1} \text{K}^{-1}$)	780
Thermal conductivity, K_c ($\text{W m}^{-1} \text{K}^{-1}$)	22
Thermal diffusivity, $\alpha \cdot 10^{-6}$ ($\text{m}^2 \text{s}^{-1}$)	6.06
Melting latent heat, h_m (J kg^{-1})	247 000
Vaporized material fraction, f_v (%)	10
Vaporization latent heat, h_v (J kg^{-1})	6 340 000
Surface tension, γ (N m^{-1})	1.880

$$Pe = \frac{\rho \cdot c_p}{K_c} \cdot \frac{r_0}{2} \cdot v, \quad (7)$$

where c_p is the specific heat capacity, ρ is the material density, r_0 is the width of the melting front, and v is the processing speed.

Finally, according to Lind *et al.*,²⁶ the maximum cutting speed achievable with a laser power P is reached when the absorbed power is no longer sufficient to melt the material volume per unit of time required to generate the cutting kerf. An estimate of this cutting speed under various processing conditions can be derived as follows:

$$v_{\text{max}} = \frac{P \cdot A - P_L}{F \cdot \rho \cdot (c_p \Delta T + h_s + f_v h_v)}. \quad (8)$$

III. MATERIALS AND METHODS

A. Material

The material employed was 1 mm thick stainless steel AISI304. Its nominal chemical composition and physical properties are summarized in Tables I and II, respectively.^{28,29}

B. Laser system

The remote fusion cutting experiments were conducted on a robotic laser system originally designed for welding applications

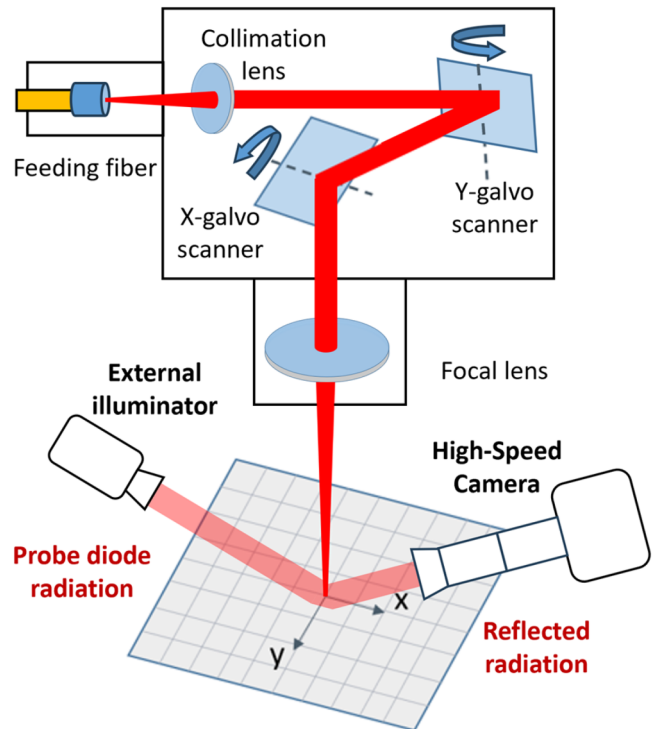


FIG. 2. Schematic representation of the experimental setup for the remote fusion cutting process with a high-speed monitoring system.

18 November 2024 10:36:43

TABLE III. Laser system specifications.

Laser cutting system	Values
Wavelength, λ (nm)	1070
Beam quality factor, M^2	11.2
Laser power, P (W)	6000
Feeding fibre core diameter, d_{core} (μm)	100
Focal length, f_{foc} (mm)	300
Collimation length, f_{col} (mm)	200
Beam waist diameter, d_{waist} (μm)	150

and subsequently adapted to perform remote separation operations (BLMGroup, Cucciago, Italy). Within the same laser system, both welding and remote cutting processes can be successfully performed. This system consisted of a 6-degree-of-freedom robotic arm and a 2-degree-of-freedom rotary/tilting table. An industrial high-power multimode fiber laser source capable of delivering up to 6 kW of power at 1070 nm (YLS-6000-CUT, IPG Photonics Corp., Oxford, Massachusetts) was employed to cut the material. The transport fiber, having a core diameter of 100 μm , was coupled to a wobble head capable of oscillating the beam in various trajectories with up to 500 Hz frequency and 3 mm amplitude (IPG D50, Oxford, MA, USA). A schematic representation of the experimental setup is shown in Fig. 2.

The optical path consisted of a 200 mm collimating and a 300 mm focusing lens producing a 150 μm beam waist diameter. Laser system specifications are reported in Table III.

Moreover, a high-speed camera and a secondary illumination light source were employed to observe the process from an off-axis perspective. The illumination light was a CAVILUX HF (Cavitar, Tampere, Finland) laser source emitting at 640 nm and synchronized with the shutter of the camera. The high-speed camera equipped with a CMOS sensor was a Fastcam Mini AX200 (Photron, Tokyo, Japan) enabling elevated acquisition rates up to 900 000 fps.

C. Experimental design

Initially, the conventional remote fusion cutting process employing linear trajectories was addressed. Previous literature publications highlighted the influence of the laser beam size on the ejection of the molten material from the kerf, which directly impacts the feasibility of material separation. Accordingly, the effect of the laser beam dimension and processing speed was experimentally evaluated in the first part of this study. The laser power

TABLE IV. Linear trajectories: experimental campaign.

Fixed parameters	
Laser power, P (W)	5000
Oscillation type	None
Variable parameters	
Spot diameter, d_{spot} (μm)	150; 214; 433; 677; 778; 877; 1028
Cutting speed, v (m/s)	0.05–0.15

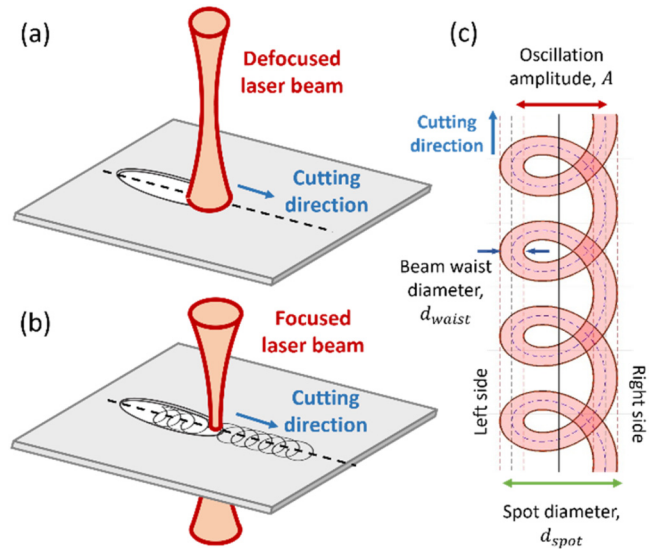


FIG. 3. Schematic representation of the remote fusion cutting process: (a) defocused laser beam on a linear trajectory and (b) focused laser beam oscillating with a circular pattern. (c) Schematic representation of a circular trajectory.

was kept fixed at 5 kW, while the focal position was varied between 0 and 10 mm above the workpiece surface. In these working conditions, the spot sizes on the material surface varied from 150 up to 1028 μm . Furthermore, 11 cutting speed levels between 0.05 and 0.15 m/s were examined, evenly spaced at intervals of 0.01 m/s. Process parameters are summarized in Table IV.

Conventional remote fusion cutting process employs highly defocused laser beams to enlarge the kerf to facilitate melt ejection. However, as an alternative solution, a well-focused and oscillating laser beam can be also used. In the second part of this study, the effect of circular laser beam oscillations was experimentally investigated. A laser beam focused on the material surface was used, while circular oscillation patterns with variable amplitudes were superimposed to the linear trajectory. A comparison between the two operating conditions is represented in Figs. 3(a) and 3(b).

The oscillation amplitudes were selected to achieve spot size dimensions on the material surface equal to the one obtained with defocused laser beams [Fig. 3(c)]. The equivalent spot diameter varied between 150 and 1028 μm , corresponding to oscillation amplitudes between 0 and 878 μm . The linear speed was varied between 0.05 and 0.25 mm/s, with intervals of 0.05 m/s. Based on a preliminary investigation, a fixed oscillation frequency value of 450 Hz was considered. Process parameters are summarized in Table V.

D. Characterization and measurement equipment

Each processing condition was replicated two times resulting in a total of 224 samples. These were visually inspected, and three categorical conditions were identified.

- No separation: the molten material is not ejected but resolidified, forming a remolten seam.

18 November 2024 10:36:43

TABLE V. Beam oscillations: experimental campaign.

Fixed parameters	
Laser power, P (W)	5000
Oscillation type	Circular
Wobbling frequency, f (Hz)	450
Variable parameters	
Equivalent spot diameter, d_{spot} (μm)	150; 214; 433; 677; 778; 877; 1028
Cutting speed, v (m/s)	0.05–0.25

- Unstable separation: the molten material is only partially ejected, leading to partial separation of the material.
- Successful separation: the molten material is ejected, leading to complete material separation.

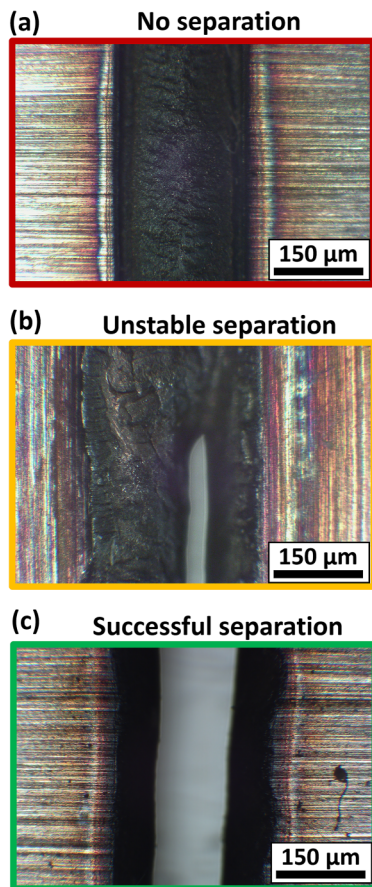


FIG. 4. Qualitative cutting results: (a) no separation (red), (b) unstable separation (yellow), and (c) successful separation (green).

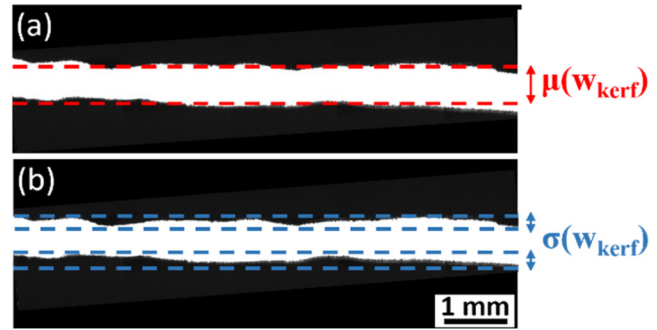


FIG. 5. Kerf profile identification via image processing algorithm. (a) Average width $\mu(w_{kerf})$ and (b) standard deviation $\sigma(w_{kerf})$.

Representative optical microscope images of these conditions are reported in Fig. 4 from a top view perspective. No separation conditions are indicated in red, while unstable and successful separations are indicated in yellow and green, respectively.

The Echo-Lab optical microscope (Echo-Lab SM 535 H, Devco S.r.l., Milan, Italy) was employed for high-resolution imaging of samples, while the kerf profile of successful conditions was analyzed through a MATLAB image processing algorithm. The top view images of the cutting kerf taken with the Mitutoyo optical microscope (Mitutoyo Quick Vision PRO ELF QV-202) were converted into binary matrices and rotated for misalignment compensation (see Fig. 5). Subsequently, the upper and lower kerf profiles were identified and the average width $\mu(w_{kerf})$ of the kerf was computed as the difference between the two [Fig. 5(a)]. Additionally, the kerf variability was determined as the standard deviation of the width profile $\sigma(w_{kerf})$ [Fig. 5(b)].

18 November 2024 10:36:43

IV. RESULTS

A. Linear cutting trajectories

Based on the previously presented analytical model (see Sec. II), the absorptivity A and cross-sectional area F are determined as a

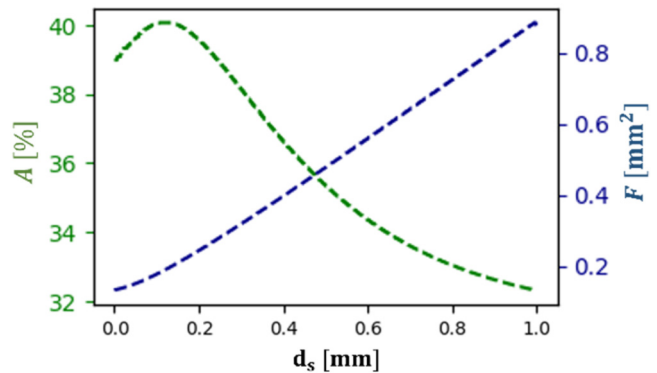


FIG. 6. Absorptivity A (in green) and cross-sectional area F (in blue), as a function of beam spot diameter on the material surface.

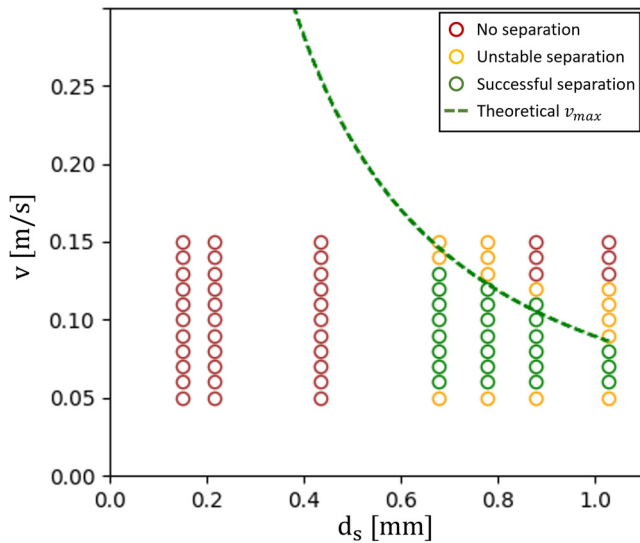


FIG. 7. Feasibility map for linear trajectory: no separation (red), unstable separation (yellow), and successful separation (green). The maximum achievable cutting speed curve, derived from the analytical model, is depicted as a dashed green line.

function of laser beam dimension on material's surface as illustrated in Fig. 6. It is evident that, as the laser beam dimension increases, the absorptivity coefficient decreases, while the cross-sectional area increases.

According to Eq. (8), these parameters have a significant impact on the maximum processing speed, which was calculated and is represented in Fig. 7, as a function of beam dimension. Additionally, Fig. 7 displays the feasibility map for linear cutting trajectory experiments, superimposed to the maximum achievable cutting speed curve derived from the analytical model.

A smaller beam allows for higher laser intensity and greater absorptivity, while also decreasing the cross-sectional area and, thus, the rate of molten material per unit time. As depicted in Fig. 7, the experimental and theoretical results demonstrated that the combined increase in absorptivity and reduction in the cross-sectional area gives the possibility to cut faster. A value of 0.08 m/s processing speed was achieved with a spot diameter of 1082 μm , whereas, with a spot of 677 μm , the speed increased to 0.13 m/s. From energetic considerations, further reducing the laser beam dimensions enables an even greater increase in the processing speed. However, the experimental results have shown that process conditions with lower spot dimensions result in failure to achieve material separation.

This is related to the fact that the beam size on the material surface is a crucial characteristic to enable molten material ejection out of the kerf. Figure 8 presents a visual comparison between the three separation conditions through high-speed video frames. The successful and unstable separation conditions correspond to beam spot diameters of 667 μm at 0.10 and 0.15 m/s processing speed, respectively [Figs. 8(a)–8(b)], while the no separation condition refers to a spot size of 150 μm and a cutting speed of 0.10 m/s [Fig. 8(c)].

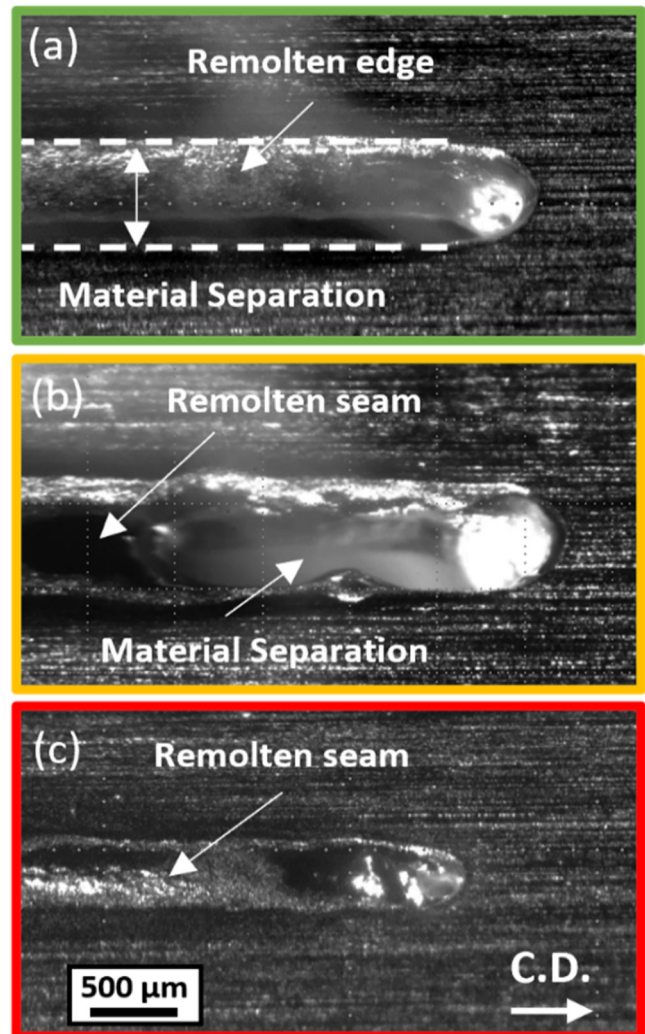


FIG. 8. High-speed video frames for (a) successful, (b) unstable, and (c) no separation conditions.

Without the blowing action of the assist gas, hydrodynamic conditions of the molten material play a significant role in the melt ejection and, consequently, on the material separation. The successful expulsion of the molten material relies on the pressure field generated by the recoil pressure, as well as material viscosity and surface tension as discussed by Hirano *et al.*³⁰ Small laser beams generate a restricted molten area, which severely limits the ejection of the molten material. This leads to the formation of an inconsistent remolten seam, ultimately resulting in a failure to achieve separation. Conversely, enlarging the laser beam enables a wider molten area, thereby enhancing melt ejection and, thus, enabling complete material separation even in the absence of the gas jet.

Furthermore, the cut quality of successful separation conditions was characterized in terms of average kerf width $\mu(w_{\text{kerf}})$ and

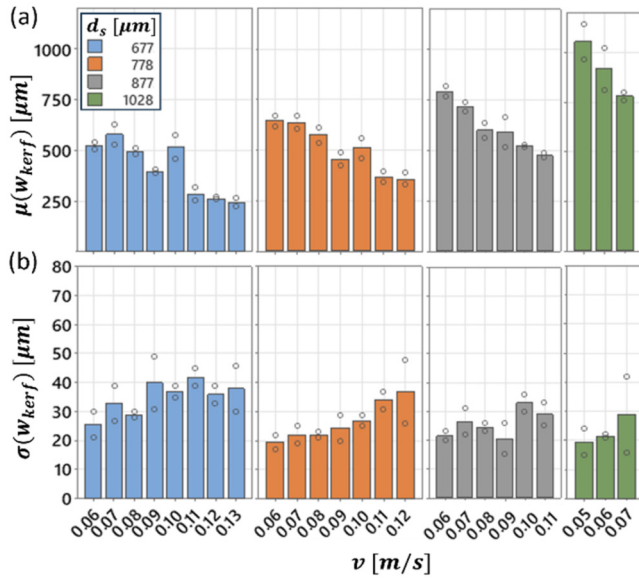


FIG. 9. Cut quality evaluation as a function of cutting speed and spot diameter for linear trajectories: (a) kerf width $\mu(w_{kerf})$ and (b) kerf variability $\sigma(w_{kerf})$.

variability $\sigma(w_{kerf})$. These are plotted in Fig. 9 as a function of cutting speed and spot dimension on the material surface. Both beam spot dimension and cutting speed have a notable impact on the kerf width and variability. Larger beam dimensions on the material surface result in a considerable widening of the kerf, whereas faster processing speeds lead to a significant reduction in the kerf width and a slight increase in kerf variability.

From Fig. 9, it is worth noticing that the kerf width is smaller than the laser spot dimensions on the material surface. This is because part of the molten material is not ejected from the kerf but remains attached to the sample cut-edges. This is evident from the high-speed video image in Fig. 8 and the sample cross sections, where the cut-edges exhibit a rounded shape caused by the

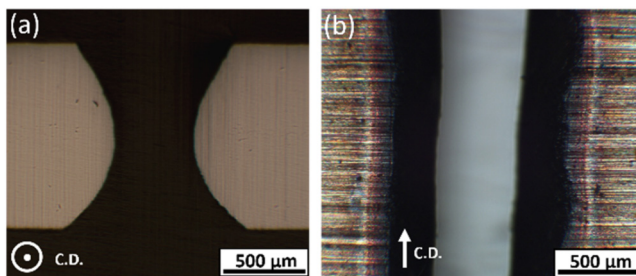


FIG. 10. Linear cutting trajectory: (a) sample cross section along the transversal direction and (b) microscope photo of the sample top surface.

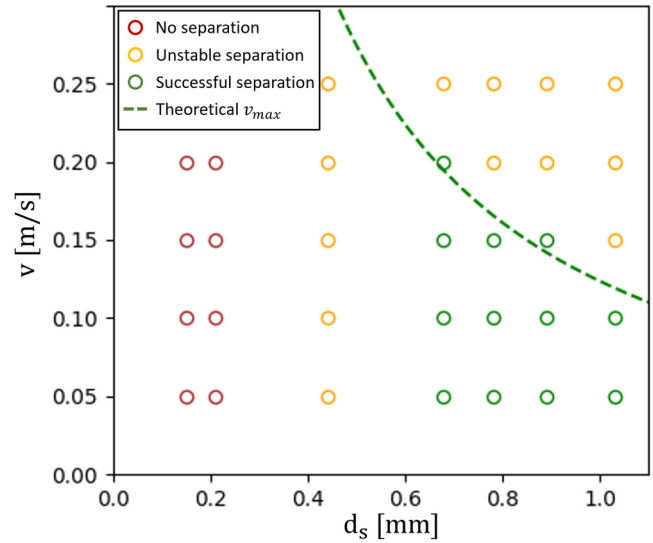


FIG. 11. Feasibility map for circular oscillations: no separation (red), unstable separation (yellow), and successful separation (green). The maximum speed curve, derived from analytical model, is depicted as a dashed green line.

resolidified material adhering to the kerf due to surface tension. An example is reported in Fig. 10(a), while the corresponding microscope photo of the kerf profile is shown in Fig. 10(b).

B. Laser beam oscillations

As already mentioned, a well-focused, and oscillating laser beam can be employed as an alternative solution to widen the kerf. This offers significantly higher absorptivity compared to a defocused beam (see Fig. 6). By selecting oscillation amplitudes to achieve a spot dimension on the material surface comparable to that of defocused beam under linear trajectory conditions [as illustrated in Fig. 3(c)], an estimate of the maximum achievable cutting speed for laser beam oscillations was retrieved. Although the molten volume is equal to the one obtained for linear trajectories, the higher absorptivity leads to a more efficient process, giving the possibility to cut faster. The feasibility map for the experiments under circular laser oscillations is reported in Fig. 11, together with the maximum achievable cutting speed curve derived from the analytical model.

The experimental results show an increase in the processing speed for all laser spot dimensions considered, consistent with theoretical findings. Specifically, the maximum achievable cutting speed could be increased from 0.13 to 0.20 m/s for 677 μm laser spot diameter.

For successful conditions, the average kerf width $\mu(w_{kerf})$ and its profile variability $\sigma(w_{kerf})$ are plotted in Fig. 12 as a function of cutting speed and spot dimensions on the material surface.

It is evident that wider laser spots on the material surface led to an expansion in the kerf dimension, while kerf variability remained unaffected by spot dimensions or cutting speed. Moreover, a notable difference between the variability of the left

18 November 2024 10:36:43

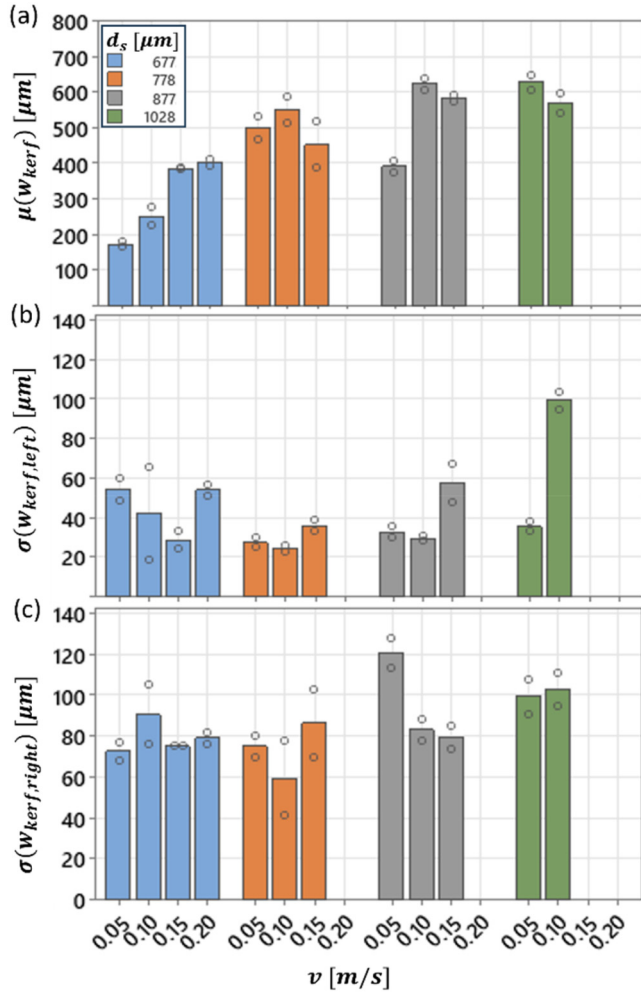


FIG. 12. Cut quality evaluation as a function of cutting speed and spot diameter for circular oscillations: (a) kerf width $\mu(W_{kerf})$; (b) left and (c) right kerf variability $\sigma(W_{kerf})$.

and right kerf profiles can be observed in Fig. 12. This difference is attributed to the circular movement of the laser beam, which significantly impacts the quality of the cut-edge profile.

In particular, the right profile exhibits significant deterioration due to the accumulation of remolten material, as highlighted in the cross-sectional image shown in Fig. 13(a). High-speed monitoring videos of the remote cutting process under circular beam oscillation [Fig. 13(b)], reveal that a portion of the molten material is not expelled downward, as in the static condition, but it is pushed backward and deposited on the right cut-edge profile.

While it is evident that circular oscillations can significantly increase the processing speed of the remote fusion cutting process, further tests and analysis are needed to ensure that they can also enhance part quality.

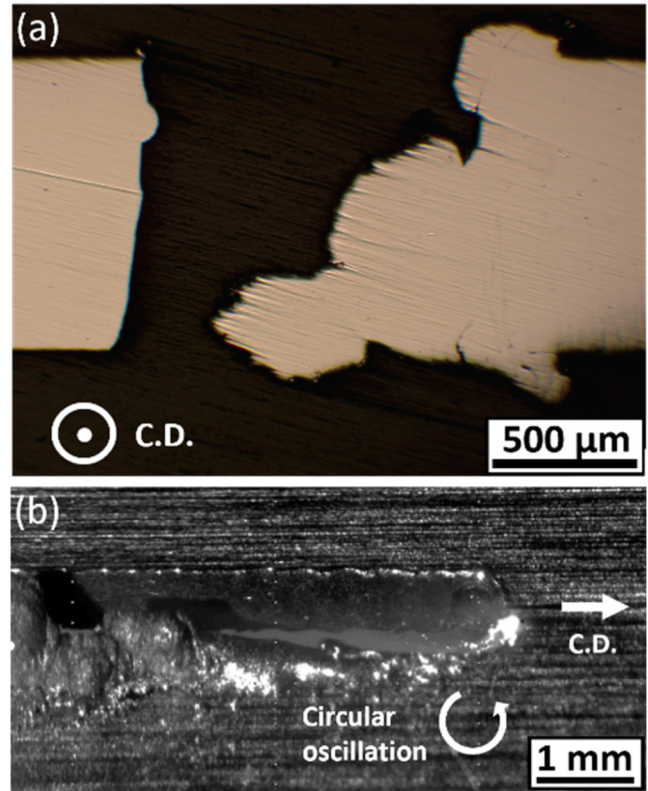


FIG. 13. Circular oscillation for a focused laser beam. Beam diameters of 677 μm and speed of 0.1 m/s: (a) cross section; (b) high-speed video frame.

18 November 2024 10:36:43

V. CONCLUSIONS

The present work explores the influence of dynamic beam shaping on the remote fusion cutting process. An analytical model based on thermodynamic analysis was developed to evaluate process performances by providing an estimate of the maximum achievable cutting speed for the remote fusion cutting process across various operating conditions.

The impact of the laser beam size on the separation process was investigated through theoretical analysis and experimentation. The results demonstrated that a smaller beam enables higher absorptivity and reduced cross-sectional areas, ultimately increasing processing speed. However, in the absence of assistant gas, the restricted molten area resulting from small laser beams severely limits the ejection of molten material. This leads to the formation of an inconsistent remolten seam, ultimately resulting in a failure to achieve separation.

Furthermore, the effect of circular laser beam oscillations superimposed on the processing feed direction was investigated. A well-focused and oscillating laser beam was employed to widen the kerf, while providing higher absorptivity compared to defocused beams. By means of circular oscillations, the results demonstrated a significant increase in the cutting speed, with a maximum rise from 0.13 to 0.20 m/s.

Future developments of the present research will be aimed at disclosing the effects of the different oscillating pattern on the process dynamics.

ACKNOWLEDGMENTS

The authors acknowledge the BLM Group for the longstanding collaboration. The Italian Ministry for University and Research (MIUR) is acknowledged for supporting the research through the National Plan for Recovery and Resilience (PNRR).

AUTHOR DECLARATIONS

Conflict of Interest

The authors have no conflicts to disclose.

Author Contributions

Matteo Busatto: Conceptualization (equal); Data curation (equal); Formal analysis (equal); Investigation (equal); Methodology (equal); Writing – original draft (equal); Writing – review & editing (equal). **Leonardo Caprio:** Conceptualization (equal); Methodology (equal); Writing – review & editing (equal). **Barbara Previtali:** Conceptualization (equal); Supervision (equal); Writing – review & editing (equal).

REFERENCES

- ¹J. P. Davim, *Nontraditional Machining Processes Research Advances* (London Springer, London, 2013). doi: 10.1007/978-1-4471-5179-1.
- ²C. L. Caristan, “Laser Cutting Guide for Manufacturing” (2003).
- ³M. F. Zaeh, J. Moesl, J. Musiol, and F. Oefele, “Material processing with remote technology revolution or evolution?,” *Phys. Proc.* **5**, 19–33 (2010).
- ⁴A. Wagner, M. Lütke, A. Wetzig, and L. M. Eng, “Laser remote-fusion cutting with solid-state lasers,” *J. Laser Appl.* **25**, 052004 (2013).
- ⁵G. F. Antonova, G. G. Gladush, A. G. Krasnyukov, F. K. Kosyrev, and N. B. Rodionov, “The mechanism of remote cutting of metals by CO₂-laser radiation,” *High Temp.* **38**, 477–482 (2000).
- ⁶G. G. Gladush and N. B. Rodionov, “Calculation of mass transfer in the remote cutting of metals by radiation of a high-power repetitively pulsed CO₂ laser,” *Quantum Electron.* **32**, 14–18 (2002).
- ⁷M. Lütke, T. Himmer, A. Wetzig, and E. Beyer, “Opportunities to enlarge the application area of remote-cutting,” in *ICALEO 2009: 28th International Congress on Laser Materials Processing, Laser Microprocessing and Nanomanufacturing, Orlando, FL, 2–5 November 2009* (Laser Institute of America, Orlando, FL, 2009), pp. 311–318.
- ⁸M. Lütke, A. Wagner, A. Wetzig, and E. Beyer, “Identification and characterization of analogies of remote fusion cutting processes using different beam sources,” in *ICALEO 2012: 31st International Congress on Laser Materials Processing, Laser Microprocessing and Nanomanufacturing, Anaheim, CA, 23–27 September 2012* (Laser Institute of America, Orlando, FL, 2012), pp. 292–301.
- ⁹A. Schober, “Experimental investigation of the cutting front angle during remote fusion cutting,” *Phys. Procedia* **39**, 204–212 (2012).
- ¹⁰S. Villumsen and M. Kristiansen, “Angular stability margins for the remote fusion cutting process,” *Phys. Procedia* **78**, 89–98 (2015).
- ¹¹A. Pihlava, T. Purtonen, A. Salminen, V. Kujanpää, and T. Savinainen, “Quality aspects in remote laser cutting,” *Weld World* **57**, 179–187 (2013).
- ¹²R. S. Matti, T. Ilar, and A. F. H. Kaplan, “Analysis of laser remote fusion cutting based on a mathematical model,” *J. Appl. Phys.* **114**, 233107 (2013).
- ¹³M. Kristiansen, S. Villumsen, and F. O. Olsen, “Modelling of the remote fusion cutting process based on experiments,” *Phys. Procedia* **78**, 110–119 (2015).
- ¹⁴A. Wetzig, P. Herwig, M. Borkmann, C. Goppold, A. Mahrle, and C. Leyens, “Fast beam oscillations improve laser cutting of thick materials: State of the art and outlook,” *PhotonicsViews* **17**, 26–31 (2020).
- ¹⁵C. Goppold, T. Pinder, P. Herwig, A. Mahrle, A. Wetzig, and E. Beyer, “Beam oscillation—Periodic modification of the geometrical beam properties,” in *Proceedings of the 8th Proceeding LiM, Munich, Germany, 22–25 June 2015* (German Scientific Laser Society, Munich, 2015), Vol. 112, pp. 1–8.
- ¹⁶C. Goppold, T. Pinder, and P. Herwig, “Transient beam oscillation with a highly dynamic scanner for laser beam fusion cutting,” *Adv. Opt. Technol.* **5**, 61–70 (2016).
- ¹⁷C. Goppold, P. Herwig, D. Stoffel, and M. Bach, “Tip-tilt piezo platform scanner qualifies dynamic beam shaping for high laser power in cutting applications,” in *Proceedings of Lasers in Manufacturing Conference, 2019* (German Scientific Laser Society, Munich, 2019).
- ¹⁸N. Levichev, M. R. Vetrano, and J. R. Dufflou, “Melt flow and cutting front evolution during laser cutting with dynamic beam shaping,” *Opt. Lasers Eng.* **161**, 107333 (2023).
- ¹⁹N. Levichev, P. Herwig, A. Wetzig, and J. R. Dufflou, “Towards robust dynamic beam shaping for laser cutting applications,” *Procedia CIRP* **111**, 746–749 (2022).
- ²⁰M. Kardan, N. Levichev, S. Castagne, and J. R. Dufflou, “Cutting thick aluminum plates using laser fusion cutting enhanced by dynamic beam shaping,” *J. Laser Appl.* **35**, 042074 (2023).
- ²¹M. Kardan, N. Levichev, and J. R. Dufflou, “Experimental and numerical investigation of thick plate laser cutting using dynamic beam shaping,” *Procedia CIRP* **111**, 740–745 (2022).
- ²²S. L. Villumsen, M. Kristiansen, and F. O. Olsen, “On the stability and performance of remote DOE laser cutting,” *Phys. Procedia* **83**, 1206–1216 (2016).
- ²³S. L. Villumsen and M. Kristiansen, “Investigation of cutting quality of remote DOE laser cutting in 0.5 mm stainless steel,” *Phys. Procedia* **89**, 164–171 (2017).
- ²⁴W. M. Steen and J. Mazumder, *Laser Material Processing* (Springer London, London, 2010), doi: 10.1007/978-1-84996-062-5.
- ²⁵A. Mahrle and E. Beyer, “Theoretical aspects of fibre laser cutting,” *J. Phys. D: Appl. Phys.* **42**, 175507 (2009).
- ²⁶J. Lind, C. Hagenlocher, N. Weckenmann, D. Blazquez-Sanchez, R. Weber, and T. Graf, “Adjustment of the geometries of the cutting front and the kerf by means of beam shaping to maximize the speed of laser cutting,” *Int. J. Adv. Manuf. Technol.* **126**, 1527–1538 (2023).
- ²⁷W. Schulz, D. Becker, J. Franke, R. Kemmerling, and G. Herziger, “Heat conduction losses in laser cutting of metals,” *J. Phys. D: Appl. Phys.* **26**, 1357–1363 (1993).
- ²⁸J. Zhou, H. L. Tsai, and T. F. Lehnhoff, “Investigation of transport phenomena and defect formation in pulsed laser keyhole welding of zinc-coated steels,” *J. Phys. D: Appl. Phys.* **39**, 5338–5355 (2006).
- ²⁹F. Dausinger and J. Shen, “Energy coupling efficiency in laser surface treatment,” *ISIJ Int.* **33**, 925–933 (1993).
- ³⁰K. Hirano, R. Fabbro, and M. Muller, “Experimental determination of temperature threshold for melt surface deformation during laser interaction on iron at atmospheric pressure,” *J. Phys. D: Appl. Phys.* **44**, 435402 (2011).